Functions of magnetic nanoparticles in selective laser sintering (SLS) 3D printing of pharmaceutical dosage forms

Yu Zhang[a], Jiaxiang Zhang[a], Rishi Thakkar[a], Amit Raviraj Pillai[a], Jiawei Wang[a], Anqi Lu[a], and Mohammed Maniruzzaman[a*]

[a]Division of Molecular Pharmaceutics and Drug Delivery, College of Pharmacy, The University of Texas at Austin, Austin, TX 78705,USA

*Corresponding author

Mohammed Maniruzzaman PhD, SRPharms.

Assistant professor

Pharmacy building, 2409 university avenue, Stop A1920, Austin, Texas 78712

Email: M.Maniruzzaman@austin.utexas.edu

Phone: +1-(512)-232-4743

Fax: +1-(512)-560-6279

1. Abstract

Selective laser sintering (SLS) 3D printing (3DP) offers novel opportunities for manufacturing various pharmaceutical dosage forms with a wide array of drug delivery systems. The purpose of this research was to introduce ferromagnetic nanoparticles, for the first time, as a multi-functional magnetic and heat conductive ingredient for 3DP tablet formulations, and further to analyze its effect on the drug release of the SLS printed tablets under a specially designed magnetic field. Optimization of tablet quality was performed by adjusting SLS printing parameters. The independent factors studied were laser scanning speed (2, 50, 100, and 200 mm/s), hatching space (13, 25, 50, 100, 300, and 2000 μm), and temperature. The responses measured were tablet weight, hardness, disintegration time (DT), and dissolution kinetics studied within the first hour. The content uniformity, chemical interaction, drug distribution, and surface morphology were tested for characterizing the printed dosage forms. It has been observed, for the drug formulations with carbonyl iron, due to its inherent heat conductivity, that sintering tablets required low energy input compared to that of other batches that contained no magnetic particles, to make the tablets of the same quality attributes. Also, under the magnetic field, printed tablets with carbonyl iron released 25% more drug as compared to those without. Therefore, we report for the first time the use of magnetic nanoparticles as a novel conductive excipient to sinter the particles in an SLS 3D printing process of pharmaceutical dosage forms and hence this finding opens up numerous opportunities for magnetically triggerable drug delivery systems.

Keywords: 3D printing, Selective laser sintering, pharmaceutical dosage forms, carbonyl iron

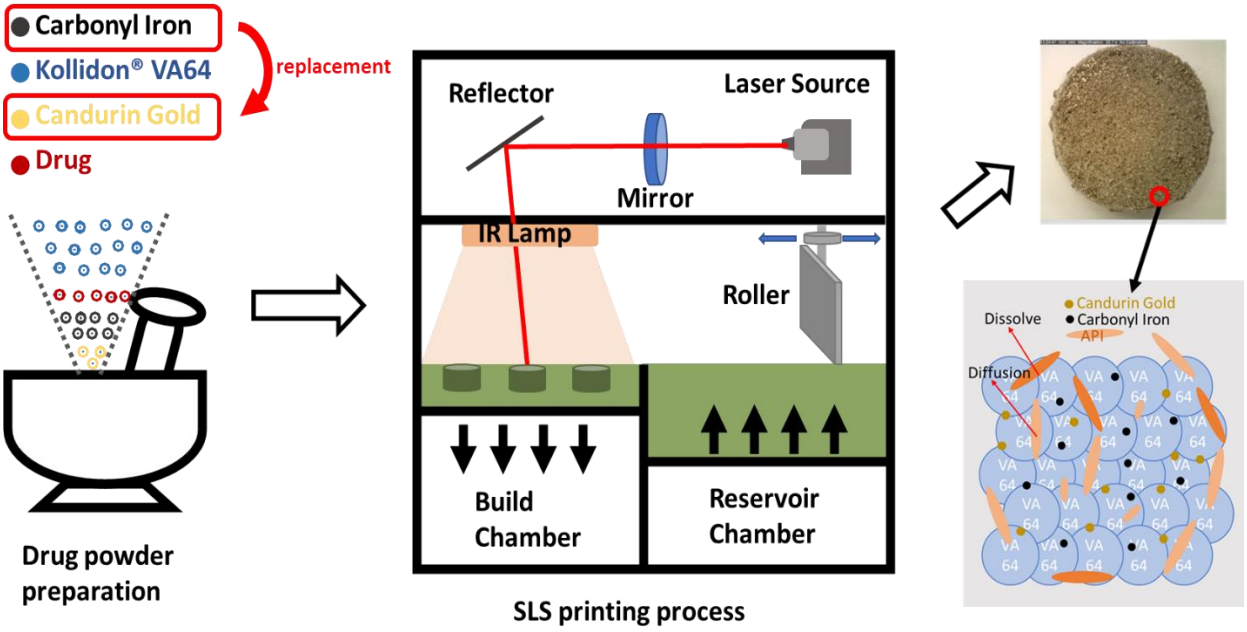

Graphical Abstract

2. Abbreviations

selective laser sintering (SLS)

three-dimensional printing (3DP)

disintegration time (DT)

fused-deposition modeling (FDM)

stereolithography (SLA)

computer-aided design (CAD)

printed tablets (PTs)

food and drug administration (FDA)

differential scanning calorimetry (DSC)

X-Ray powder diffraction (XRPD)

Fourier transform infrared (FTIR)

polarized light microscopy (PLM)

scanning electron microscopy (SEM)

United States pharmacopeia (USP)

3. Introduction

With the introduction of 3D printing in pharmaceutical sciences, many types of 3D printing techniques have been used in this area, such as fused-deposition modeling (FDM) (1) (2), stereolithography (SLA) (3)(4), and injection molding (5)(6). In the past five years, the selective laser sintering (SLS) 3D printing technique for making personalized dose and dimension-specific dosage forms has gained widespread attention (7)(8)(9). This innovative 3DP technology offers the possibility of manufacturing medicines utilizing a laser beam to selectively sinter powder material together, which subsequently solidifies to form 3D objects with the assistance of a computer-aided design (CAD) software (10)(11).

In the early 1980s, Carl Deckard and Joe Beaman invented the first SLS printer. It was based on a neodymium-doped yttrium aluminum garnet laser, which had a power of 100 W (12). Then, the SLS printing technique was well known for its successful applications in manufacturing metal parts (13), implants (14)(15), and tissue scaffolds (10). SLS printing shows its advantages in the pharmaceutical field for its solvent-free printing process with relatively high fabrication speed. This method does not require a filament of raw ingredients, is not limited by polymerizable monomer materials, does not need post-processing, and has no requirement for a liquid binder. Due to the solvent-free process, water and organic solvent sensitive drugs can add to the powder formulations. What's more, the printed tablets (PTs) are directly available for consumption after printing since no requirements for post-processing steps such as drying or curing except collecting the PTs from the loose powder. Last but not least, various drug release types of the PTs can

be made by simply adjusting the drug formulations (mainly depends on dispersion polymer) and manipulating printing process parameters (e.g., laser scanning speed, hatching speed, temperature et al.). The main disadvantage of SLS printing technology is the requirement of thermoplastic materials and the possibility of drug and excipient degradation by the laser and pre-warming.

Carbonyl iron particles have magnetism, moving in different directions by adjusting the magnetic field (16). It also has high oxidation resistance and is a good conductor of heat (17). Furthermore, it is also an FDA approved human iron supplement (18)(19). By using SLS to fabricate PTs, a wavelength absorbent is essential for the powder formulation. Candurin® Gold sheen (Potassium aluminum silicate, iron oxide, Titanium dioxide TiO_2) was the most commonly used absorbent (20)(21). Even though it is an FDA approved color additive (US hazard communication standard 21 CFR part 73: section 73.1350), the maximum usage lever is 3 % by weight of the finished product or ingested drug. As laser absorption agents, a minimum of 3 w/w% of candurin® gold sheen was used to help sinter a stable tablet with good hardness. This minimum amount already reaches the safety limitation, and it will be better to use less and replace it with other additives. In this study, we are making an advanced formulation for SLS PTs, which contains carbonyl iron particles for three reasons: firstly to use its magnetic property to enhance drug release; Secondly to use its good conductivity for supporting the sintering process; Thirdly, as an iron supplement for daily health care.

4. Materials and Methods

4.1. Materials

Isoniazid (⩾99% TLC, analytical standard, Sigma-Aldrich, USA) was used as a model drug (Molecular weight 137.14 g/mol, melting point 171-173 °C). Kollidon® VA64 is a vinylpyrrolidone-vinyl acetate copolymer, kindly donated by BASF, USA. Carbonyl Iron (⩾97% Fe basis, Particle size 5-50 µm) was purchased from Sigma-Aldrich, USA. Candurin® Gold Sheen was purchased from Merck, Germany.

4.2. Methods

4.2.1. Selective Laser Sintering Process

The desktop SLS printer (Sintratec Kit, AG, Brugg, Switzerland) was used to print the oral dosage forms. 3D builder (version 18.0.1931.0, Microsoft Corporation) was used to design the templates of the solid dosage forms (11.15 mm diameter and 3.75 mm height cylinder tablets).

Preparation of the physical drug mixture, 5% Isoniazid (≥99% TLC, analytical standard, Sigma-Aldrich, USA) was used as a model drug (Molecular weight 137.14 g/mol, melting point 171-173 °C). Kollidon® VA64 (BASD, USA), a vinylpyrrolidone-vinyl acetate copolymer, was selected as a polymeric carrier (Tg = ~105 °C). Candurin® Gold Sheen (3% w/w) and carbonyl iron (5% w/w) were added to the formulations. For all the formulations, 200 g of a mixture of the model drug and excipients were blended together using a mortar and pestle. All the powders were sieved using a 500 µm sieve to permit a better flow of the powder particles and transferred to the powder reservoir compartment (110x110x110 mm) of the SLS printer.

During the printing process, the powder was spread like a layer of 0.15 mm by the roller and sintered by a 2.3 Watt blue diode laser (445nm) at a selected scanning speed. The tablets were formed by sintering the powder layer-by-layer based on the designed STL file. After the printing process, the printer was cooled down. The tablets were collected from the powder bed after removing the loose powder.

4.2.2. Thermal Analysis

Differential scanning calorimetry (DSC, DSC Q20, TA® instruments, New Castle, DE, USA) analysis was used to characterize the pure active pharmaceutical ingredient (API), polymer, API-polymer physical mixture and the crushed powder of printed tablets. Approximately 7-12 mg of samples were weighed in standard DSC aluminum pans and sealed with standard aluminum lids (DSC consumables incorporated, Austin, MN, USA) using a calibrated balance. The prepared samples were subjected to a heat-cool-heat ramp circle heated from 10 °C to 200 °C with a ramp rate of 10 °C/min. A purge gas (Nitrogen) at a flow rate of 50 mL/min was used for all the experiments. The data were collected by TA advantage software (Q series, Version 2007 build 13029.20308) and analyzed by TA instruments Universal Analysis 2000. The results were presented as a plot of temperature (°C) versus reverse heat flow (mW).

4.2.3. X-Ray Powder Diffraction (XRPD) Studies

XRPD instrument (MinFlex 600, Rigaku Corporation, Tokyo, Japan), Cu Kα X-ray source (λ = 1.5418 Å), was used for obtaining X-ray powder diffraction patterns of pure active pharmaceutical ingredients (API), polymer, carbonyl iron, API-polymer physical mixture, and the crushed powder of printed tablets. The prepared samples were loaded onto the magnetic sample cell and placed in the sample holder of the benchtop XRPD instruments separately. The samples were scanned from a 2θ angle of 10 to 85 degrees, with a

stepwise size of 0.02 degrees at a speed of 5°/min. The current and voltage applied were 15 mA and 40 kV, respectively. Collected data were presented as a plot of 2θ (degree) versus intensity (a.u.) and analyzed.

4.2.4. Fourier Transform–Infrared (FTIR) Spectroscopic Analysis

Fourier Transform Infrared (FTIR) spectra of the API, polymer, Candurin® Gold Sheen, API-polymer physical mixture, and the crushed powder of printed tablets were collected using a modular Nicolet™ iS™ 50 FTIR system (ThermoFisher Scientific, Waltham, Massachusetts, USA). 20-25 mg of samples were analyzed for percentage transmittance from 4000 to 400 cm^{-1}, at a resolution of 4 cm^{-1} and 64 scans per run. The absorbance mode was used. OMNIC™ series software (Version 9.0 ThermoFisher Scientific, Waltham, MA, USA) was used to capture and analyze the spectra.

4.2.5. Determination of Tablets Morphology

A VWR® digital caliper (VWR®, PA, USA) was used to measure the diameters and height of the tablets. Images of the tablets were taken by using Dino-Lite optical microscopy.

4.2.6. Polarized Light Microscopy (PLM)

Olympus BX53 polarizing photomicroscope (Olympus America inc., Webster, TX, USA) was used to observe the structure of the physical mixture, model drug, polymer, and crushed printed tablets. The PLM was also assembled with a self-built heating system to analyze the influence of temperature on the drug powder. QICAM Fast 1394 digital camera (Qimaging, BC, Canada) was used to capture the images, and data were analyzed by Linksys 32 software® (Linkam sci ins Ltd., Tadworth, UK)

4.2.7. Scanning Electron Microscopy (SEM)

Scanning electron microscopy (Quanta FEG 650 ESEM, FEI Company, Hillsboro, OR, USA) was employed to observe the surface and cross-section of the printed tablets. The

199 samples were first coated with gold by vacuum sputtering (EMS Sputter Coater, Hatfield,
200 PA, USA) before observation under SEM. Microscope images were captured at a working
201 distance of ~9 mm, an accelerated voltage of 5 kV, and an emission current of 15 µÅ.
202 The SEM with embedded energy dispersive X-ray (EDX)

203 **4.2.8. Texture Analysis**

204 The hardness of printed tablets was determined using a TA-XT2 analyzer (Texture
205 Technologies Corp, New York, NY, USA).

206 **4.2.9. Disintegration**

207 USP disintegration equipment (Vankel Varian VK-100, NC, USA) was used to determine
208 the disintegration time of the printed tablets. Printed tablets were gently placed on the
209 surface of a petri-dish containing 900 mL of 0.01M HCl solution at 37 ± 0.5°C. All the
210 measurements were done in six replicates.

211 **4.2.10. Dissolution**

212 Drug dissolution profiles for the formulations were obtained with a United States
213 Pharmacopeia (USP)-II dissolution apparatus (Vankel-Varian VK 7000 dissolution system,
214 Varian, Inc., Cary, NC, USA). The dissolution was performed in 900 mL of hydrochloric
215 acid (HCl)-potassium chloride (KCl) buffer (pH 2, 0.1 M) at 50 rpm and 37 ± 0.5°C.
216 Samples (1ml) were collected at 5, 10, 15, 20, 30, 45, and 60 min, and 10 µL of the
217 sample was injected into the HPLC (Agilent 1100 series., Santa Clara, CA, USA) system
218 to determine the amount of the dissolved drug at 283 nm. The collected data were
219 analyzed using Agilent ChemStationsoftware (version C.01.03, Agilent Technologies, Inc.,
220 Santa Clara, CA, USA)

5. Results and discussion

5.1. Morphology and mechanical property of the printed tablets (PT)

SLS printers use laser energy to selectively fuse powder particles together and form 3D objects with the aid of a computer-aided design (CAD) model (22)(23)(24). In the preliminary experiment, the thermoplastic excipients Kollidon VA64, 5 wt% isoniazid, 5% carbonyl iron, and 3 wt% Candurin Gold Sheen were initially tested to evaluate their printability by using an SLS 3D printer. For the formulation of the model tablets, Candurin Gold sheen is a pharmaceutical pigment; here, it is used as an absorbent to yield an optimum sintering process because it absorbs radiation at the wavelength of the laser (445nm) (25)(20). Carbonyl iron is an FDA approved iron supplement (Code of Federal Regulations CFR Title 21); it was added to the formulation due to its oxidation resistance property, a good conductor of heat, and its magnetic property. Kollidon VA64 is a pharmaceutical excipient polymer with fast disintegration properties (26)(27). Isoniazid is the model active pharmaceutical ingredient (API).

The desired sintered tablets can be obtained by mainly controlling the internal temperature of the SLS printer, the laser scanning speed, the hatching spacing (the distance between interior hatching lines), and formulation compositions (27)(24). Before the SLS printing, the 3D files of each design was converted into the described software (Sintratec central 1.2.4, USA). The layer thickness, which is the distance between the layers in the vertical distance, was set to 150 µm.

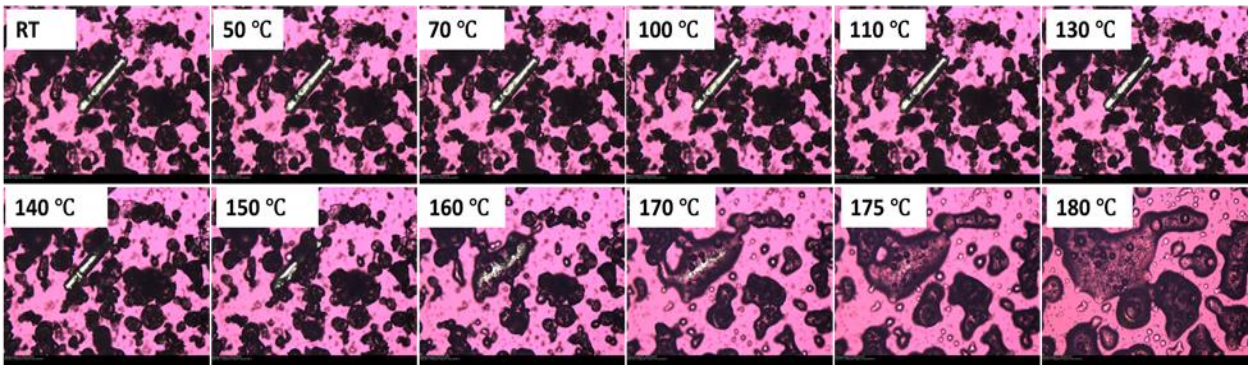

Figure 1. PLM micrographs of the physical mixture of drug powder from room temperature (RT) to 180 °C.

The internal temperature depends on the glass transition temperatures of the excipient polymers (Kollidon® VA 64 *Tg*= 98 ~ 108 °C) and the melting point of the model drug (Isoniazid Tm= 171 ~ 173 °C) (shown in Figure 1 and Figure 6). Figure 1 shows that the polymer starts to melt at 100 °C then the crystal drug from 100 °C to 160 °C. When the temperature is over 160 °C, the isoniazid crystal drug melted and mixed with the melted polymer in the end (shown in Figure 1). In this experiment, the polymer used in the SLS printed tablets formed by sintering the powders should not melt during the printing process. Thus, the temperature of the powder surface should not be over 98 °C (minimum *Tg* of Kollidon® VA64). Also, the laser sintering process would give extra energy to the powder bed and increase the surface temperature of the printed tablets, so the pre-heating temperature should be 10 °C to 40 °C less than the 98 °C. The suitable temperature range was from 58 °C to 88 °C, and we chose 65 °C based on the batch size (6 tablets per batch) and the optimized heating time. Both parameters (layer thickness/temperature) were selected after an optimization process to fabricate a robust structure and were maintained throughout the printing of all the formulations.

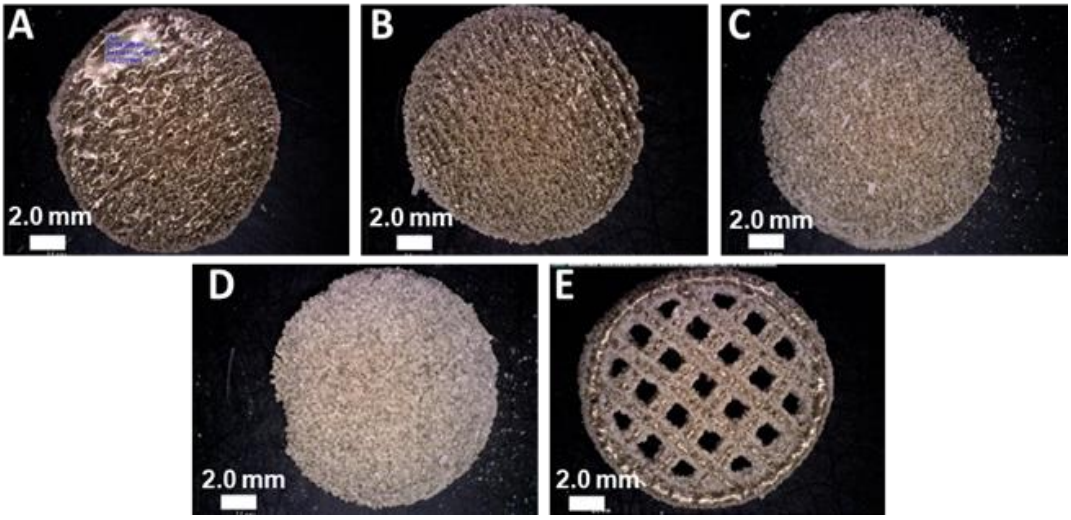

Figure 2. Digital optical microscope images of ideal printed tablets, sample printing parameters were A) LSS 10 mm/s; HS 50 µm, B) LSS 20 mm/s; HS 50 µm, C) LSS 10 mm/s; HS 100 µm, D) LSS 10 mm/s; 300 µm, and E) LSS 2 mm/s, HS 2000 µm. The diameter of the printed tablets was designed as 11.15 mm. The temperature was 65 °C.

Figure 2 shows the ideal samples of printed tablets and demonstrates the cylindrical constructs were successfully produced. All the samples were dark green due to the yellow Candurin® pigment and grey carbonyl iron. In this study, the laser scanning speed and hatching space are the two processing parameters that significantly influence the printed tablets. By reducing the laser scanning speed and hatching spacing, a longer interaction time between the powder particles and the laser beam leads to the higher transmission of energy, hence producing denser tablets. On the contrary, by increasing laser scanning speed (LSS, mm/s) and hatching space (HS, µm), less energy is transmitted, resulting in the production of weaker and more porous structures in tablets (shown in **Figure 2**). However, the decrease in scanning speed and hatching space should not exceed the recommended limit. **Figure 2**A shows that low scanning speed with tight hatching space results in thermal deformations. Furthermore, **Figure 2**E shows that a large hatching space leads to incomplete sintering. Providing sufficient energy for the adequate bonding

of the consecutive printing layers while maintaining the desired shape and dimensions of the printed tablets are essential.

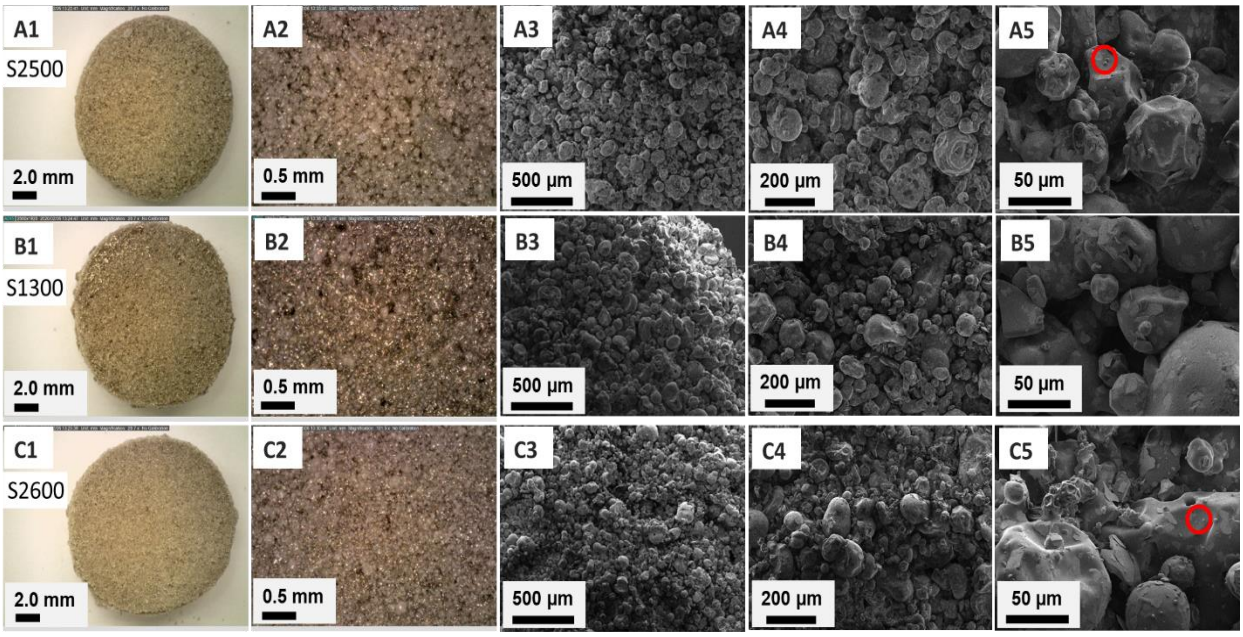

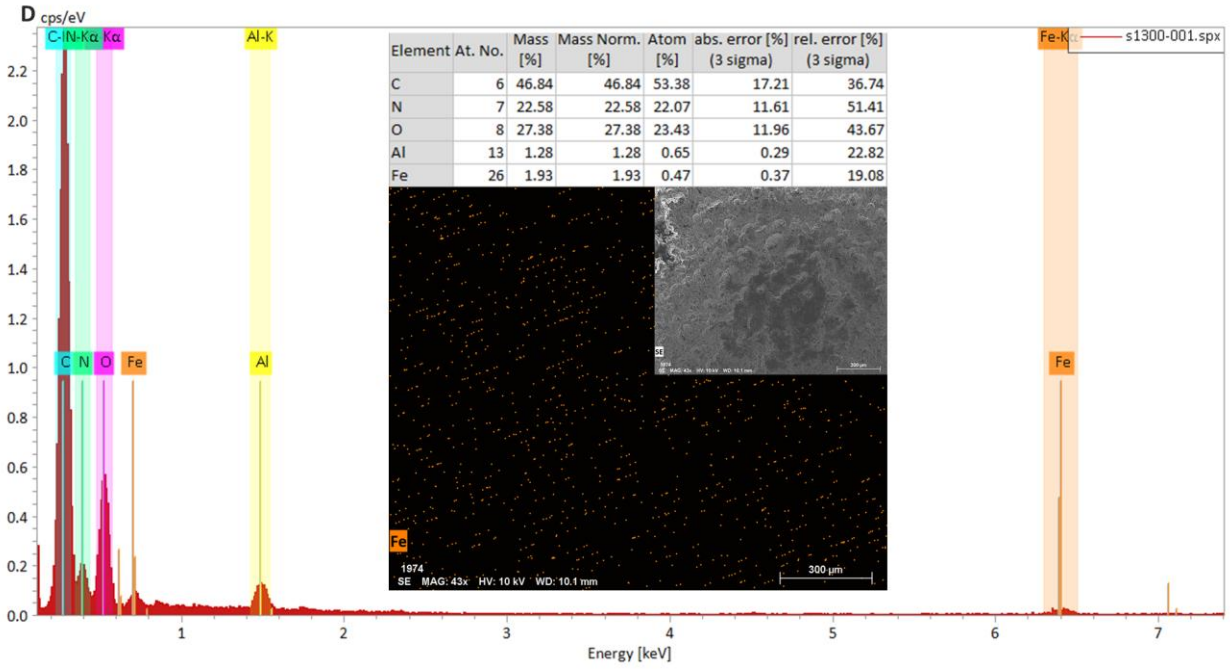

Figure 3. Dino digital microscope images (No.1 and 2) and SEM images (No.3-5) of the printed tablets. Printing parameters for each of the samples were A) LSS 100 mm/s; HS 25 µm, B) LSS100 mm/s; HS 13 µm, C) LSS 200 mm/s; HS 13 µm. The magnification of the SEM images was 50 (No.3), 100 (No.4), and 500 (No.5), respectively. D) The EDX analysis of the ideal S1300 tablet

290 **Table 1**: The characteristics of the printed tablets

	Laser Scanning Speed (mm/s)	Hatching Space (μm)	Weight (mg)	Density (mg/cm^3)	Hardness （kg）	Work of Failure (kg·sec）	Tensile strength （Kpa）	Disinteg-ration Time
S2500	100	25	172.3 ± 19.6	451.7 ± 29.2	0.1 *	15.5 *	14.9 *	≤ 1 min
S1300	100	13	224.5 ± 26.2	563.7 ± 46.6	1.9 ± 0.5	33.8 ± 10.2	284.3 ± 32.6	≤ 2 min
S2600	200	13	151.0 ± 17.8	418.6 ± 30.9	0.1 *	7.9 *	14.5 *	≤ 1 min

* Hardness values were too low to be detected

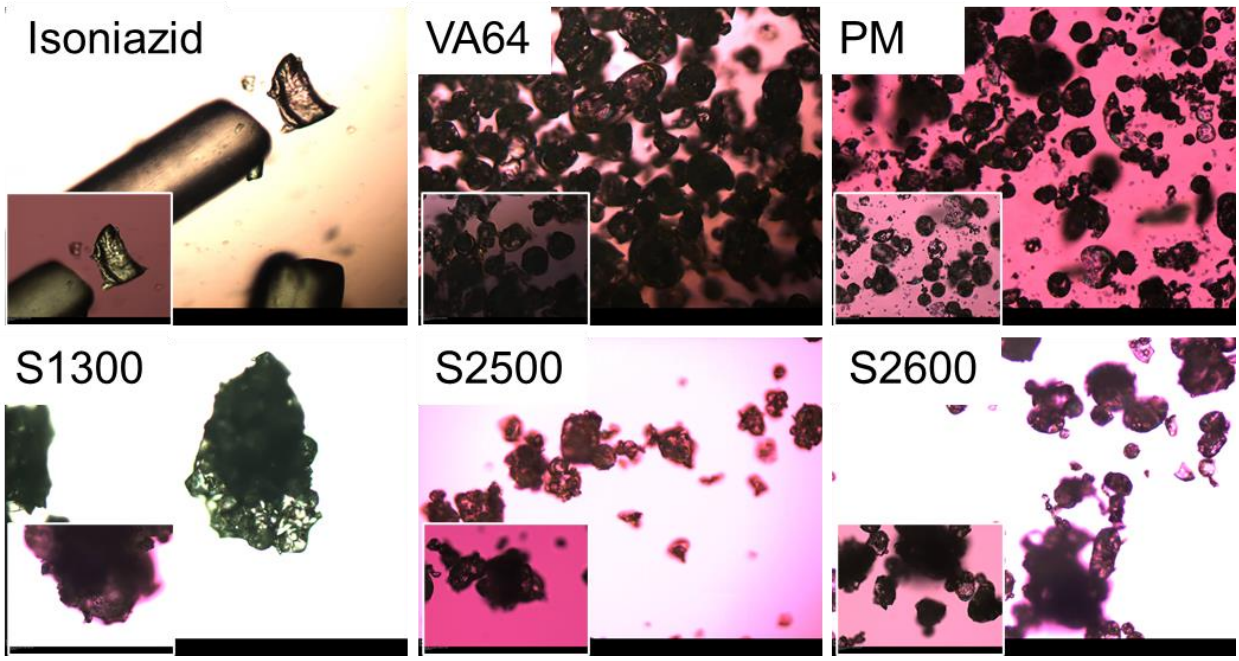

291

292 **Figure 4.** PLM microscope images of isoniazid, VA64, physical mixture of drug powder, the
293 crushed powder of printed tablets S1300, S2500, and S2600.

294

295 **Figure 3** shows the 3 cases of the ideal printed tablets for the studied powder formulations,
296 which are named S2500 (LSS 100 mm/s; HS 25 μm), S1300 (LSS 100 mm/s; HS 13 μm),
297 and S2600 (LSS 200 mm/s; HS 13 μm), respectively. Table 1 listed the printing process
298 parameters and physical properties of S2500, S1300, and S2600. The laser scanning

speed of S2600 was 2-fold higher as compared to S2500 and S1300, while the hatching space of S2500 was 2-fold higher than S2600 and S1300. Thus, S1300 had lower LSS and HS, which resulted in higher weight, density, and hardness as compared to S2500 and S2600 (shown in Table 1). By comparing S2500 and S2600, it showed that the LSS of S2500 was half that of S2600, while the HS observed for those particular tablets was the other way round. However, the weight, density, and hardness of S2500 were similar to S2600. This demonstrated that the final physical property of the printed tablets was determined by the combination of all the printing parameters. Even different printing parameters can result in similar 3D structures.

SEM images in **Figure 3** provided a visual observation of the morphology of the printed tablets and confirmation of the sintering processes in the polymer formulations. **Figure 3**A3, B3, and C3 show that S2500, S1300, and S2600 have a similar porous structure. Then by comparing 500x magnified SEM images of those samples, both S2500 and S2600 showed iron particles on the surface of the mixture powder (shown in **Figure 3** A5 and C5, in red circle), while S1300 produced a smoother surface than the other two without the iron particles which can be noticed. This phenomenon has been observed in **Figure 1**. It can be explained as the sintering energy for S1300 was adequate for the polymer to swell, relax, and melt. Then the melted polymer gets absorb onto the surface API and iron particles in Figure 4, which supports the hypothesis. By comparing the PLM images of PM and crash samples of S1300, S2500, and S2600 tablets, only S1300 shows the strong sintering structure while S2500 and S2600 show the structure which is similar to PM. In this way, under the magnetic field, the carbonyl iron goes through the polymer

particles and may induce a fast drug release. Thus, the printing parameters of S1300 were selected to print the magnetically stimulated tablets for the further dissolution study.

5.2. Physicochemical characterization of PT

FTIR spectroscopy was performed to characterize isoniazid, Kollidon VA64, and the interaction between the physical mixture and sintered PT. FTIR spectra were recorded in 700-4000 cm^{-1}. The red vertical dash line is labeled 1400 cm^{-1} to identify the fingerprint region. Polymer Kollidon® VA64 (**Figure 5**. Sixth yellow) showed a characteristic peak at 2933 and 2858 cm^{-1} due to the aliphatic C-H stretch. The peak seen at 1460 cm^{-1} is due to the C-N stretching of the pyrrolidine group, and the peak at 1730 cm^{-1} is due to the O-C=O stretch. In **Figure 5**, the brown line was used for the qualitative investigation of isoniazid by its FTIR spectra. The ring C=C has conjugated further represented by a band at about 1555 cm^{-1}. The peak is seen at 3110, and 3100-3000 cm^{-1} is due to asymmetric C-H stretch. Candurin Gold sheen did not show any peak at 4000-1400 cm^{-1}, but it offers a more substantial peak at 1000 cm^{-1} due to nitro or fluoro compound. No recognizable peak was observed for carbonyl iron as iron is not IR active. Physical mixture samples showed an additive spectrum encompassing characteristic peaks of major components, especially Kollidon® VA64. Spectrums of S1300, S2500, and S2600 were similar to the physical mixture powder, which indicated no chemical interactions during the printing process (Shown in **Figure 5**, top four). Also, Kollidon® VA64 did not degrade.

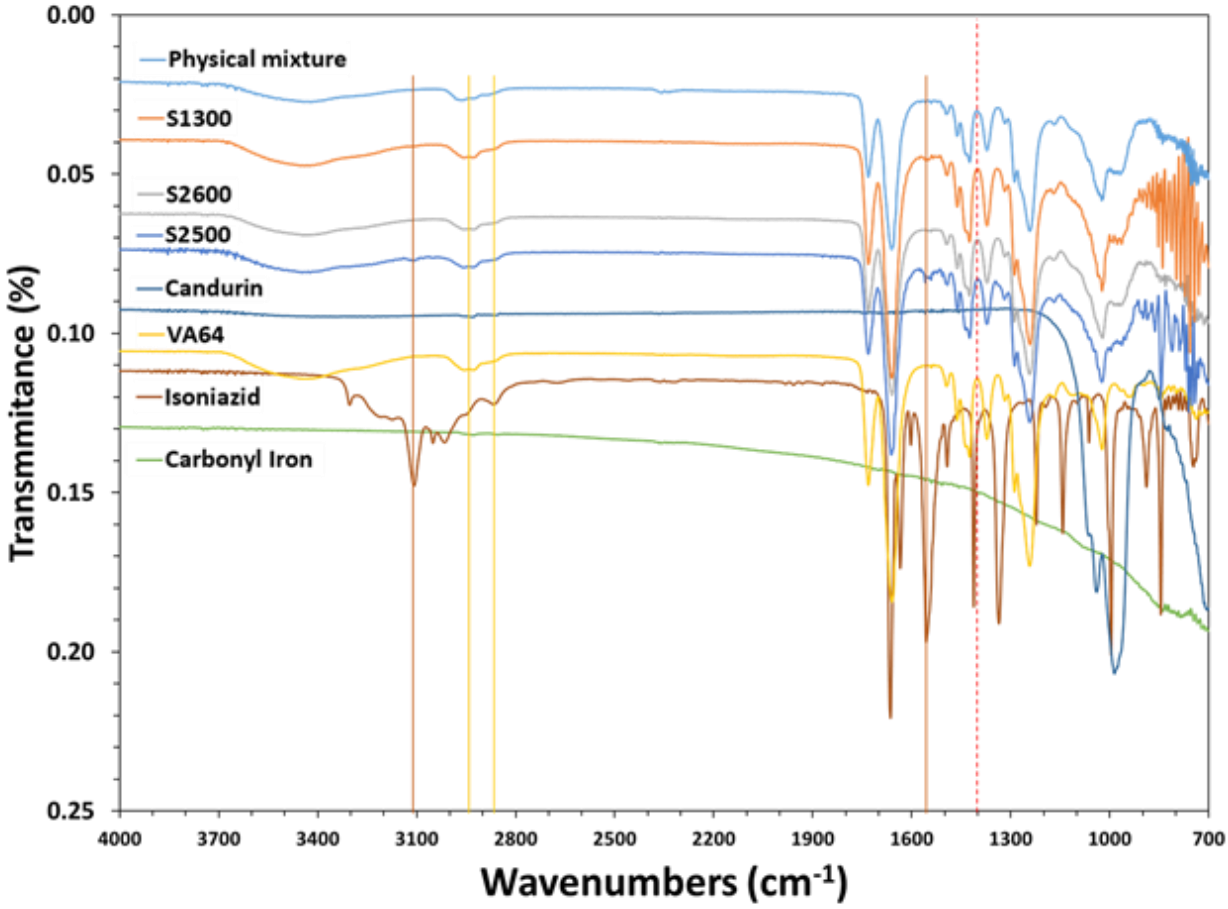

Figure 5. FTIR spectra of pure isoniazid, carbonyl iron, Kollidon VA64, Candurin gold sheen, and mixtures prior to printing and the different PT formulations. From top to bottom, first to eighth spectra are a physical mixture, S1300, S2600, S2500, Candurin gold sheen, VA64, isoniazid, carbonyl iron, respectively. Red dash line labeled the fingerprint region peat at 1400 cm^{-1}.

DSC and XRPD analysis of the drug, polymers, and mixed materials before printing and of the sintered tablets were performed to study the solid-state of the drug phase as well as the degree of magnetic iron incorporation in the polymers (shown in **Figure 6** and **Figure 7**). **Figure 6** demonstrated that the isoniazid raw ingredient exhibited a melting endotherm at approximately 172.7 °C correspondings to its melting transition. The DSC data of the physical mixture shows a small peak at 173 °C. In comparison, the sintered tablets showed no evidence of a melting endotherm at 172 °C, which means the model

drug was either molecularly dispersed within the excipient or dissolved in Kollidon VA64 due to the fusion generated during the printing process. The x-ray powder diffractograms showed an identical Fe peak at 45 °C in the sintered tablets and were confirmed by the presence of carbonyl iron (shown in **Figure 7**) due to the absence of drug peaks.

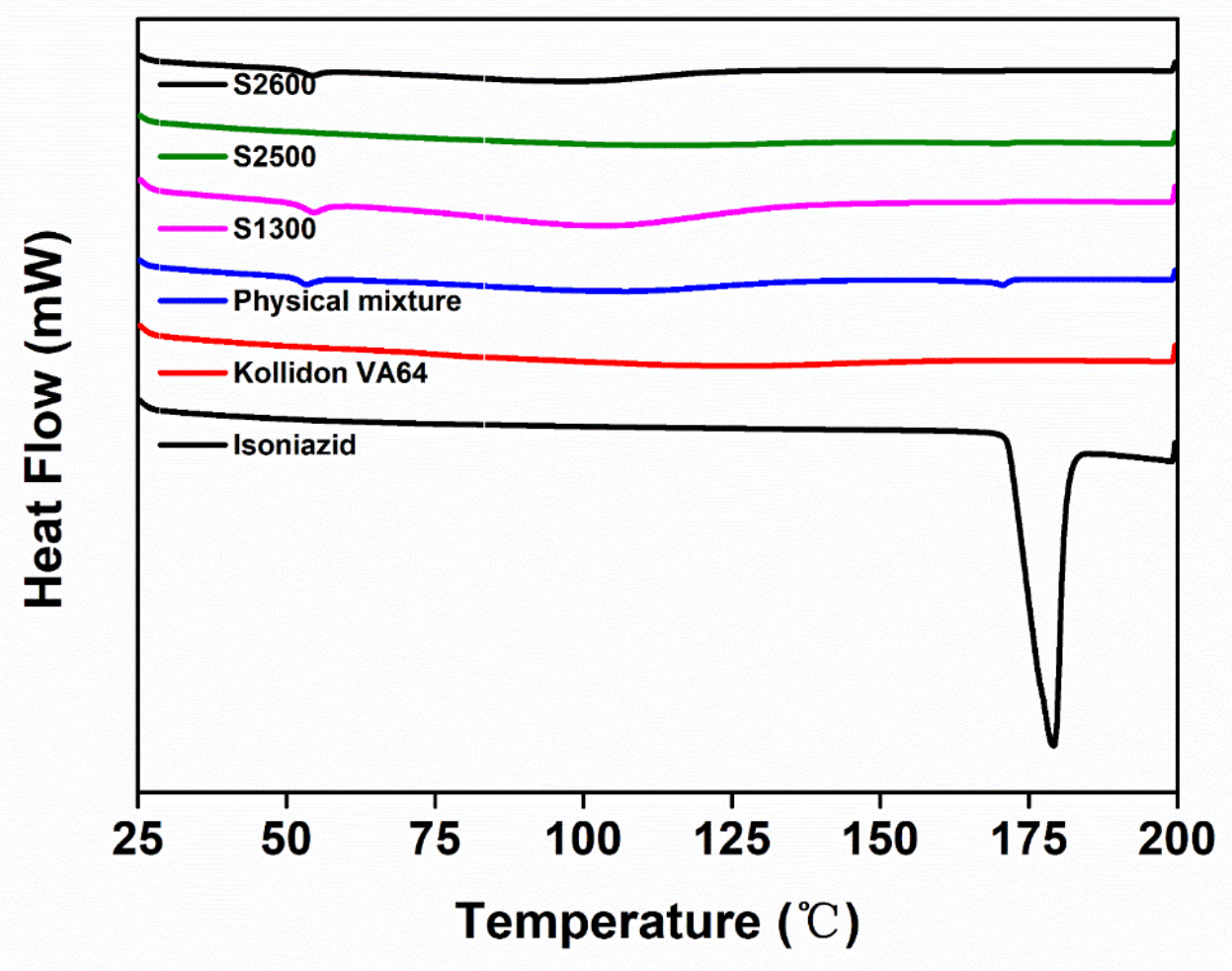

Figure 6. DSC thermograms of pure isoniazid, Kollidon VA64, and mixtures prior to printing and the different printlet formulations.

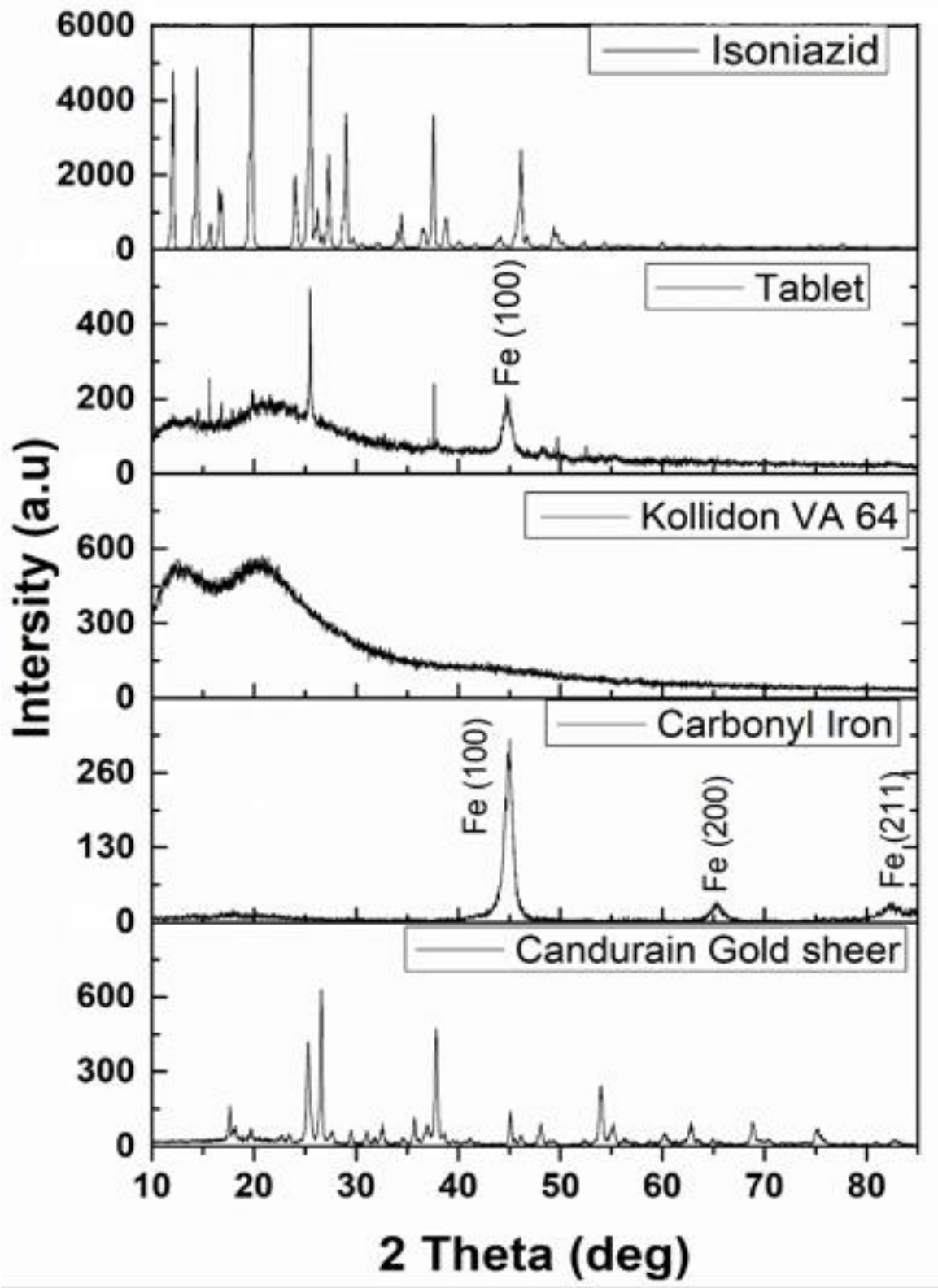

Figure 7. X-ray diffractograms of isoniazid, sintered blank tablets, sintered iron tablets, excipient polymer (Kollidon VA64), carbonyl iron, and Candurin gold sheen.

5.3. Dissolution kinetic studies

In this study, a special apparatus was designed for adding a tunable magnetic field to the standard dissolution system. **Figure 8** shows the schematic of the designed apparatus. Two round neodymium magnets (NM) were stuck on the stirring paddle, which generated a changeable magnetic field during the experiment. The surface field is about 5233 gauss. The square NM was stuck on the bottom of the beaker and used to attract the PT. The surface field is appropriately 1624 gauss. The square NM is important as, without it, the PT will be attracted by the round NM. In that situation, no changeable magnetic field stimuli were felt by the PT.

Drug dissolution characteristics of the PT were tested using a dynamic in vitro model, which simulates gastric conditions. Figure 9 shows the dissolution profiles of Kollidon VA64 based PT. In **Figure 9**A, by comparing S1300 and S2500, it was found that by increasing the hatching space from 13 to 25 μm, S2500 released 60 ± 7% of the drug in 5 mins while S1300 only released about 47 ± 5%. By increasing laser scanning speed from 100 mm/s (S1300) to 200 mm/s (S2600), S2600 had a notably shorter dissolution time. In **Figure 9**B, at the beginning of 15 minutes, without a magnetic field, S1300 PT released more drugs than S1300 under the influence of the magnetic field. This is due to the square NM attracted to the iron particles and locked the PT at the bottom, which slowed the releasing process. Then after 15 mins, S1300 PT with MF had a notable increase in the drug release amount, with drug release up to 90% in one hour. Based on the SEM images in **Figure 3**, S1300 samples showed that the carbonyl iron particles were contained inside the polymer particles. The tablets were prepared in a way that made some parts of API dissolve in the polymer. Some parts of API were inlaid on the surface

of the polymer matrix (in amorphous states), and some API got attached to the polymer surface (in crystalline forms). When the tablets came in contact with the dissolution media, regardless of the magnetic fields, the tablets disintegrated. However, the magnetic field attracts the tablets to the bottom of the vessel and slows down the disintegration, explained in the first 20 min curve in **Figure 9**B. When the tablets completely disintegrated, Kollidon® VA64 swelled and formed a hydrogel or suspension, which in turn controlled the drug release rate by diffusion without the magnetic field. Under the influence of a magnetic stimulus, the iron particles pass through the polymers and generate a microporous structure in PT, which accelerates the drug release and finally results in a higher drug release percentage than the PT without MF (explains the curve after 20 mins)

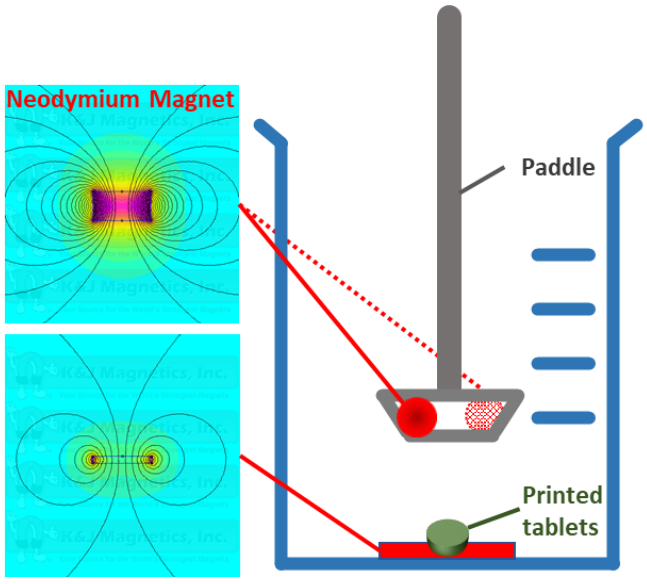

Figure 8. Schematic representation of the magnetic field added to the dissolution system. Round neodymium magnets are 0.5 inches in diameter and 0.2 inches in thickness. The square magnet is a 1-inch side with 1/8 inch thickness.

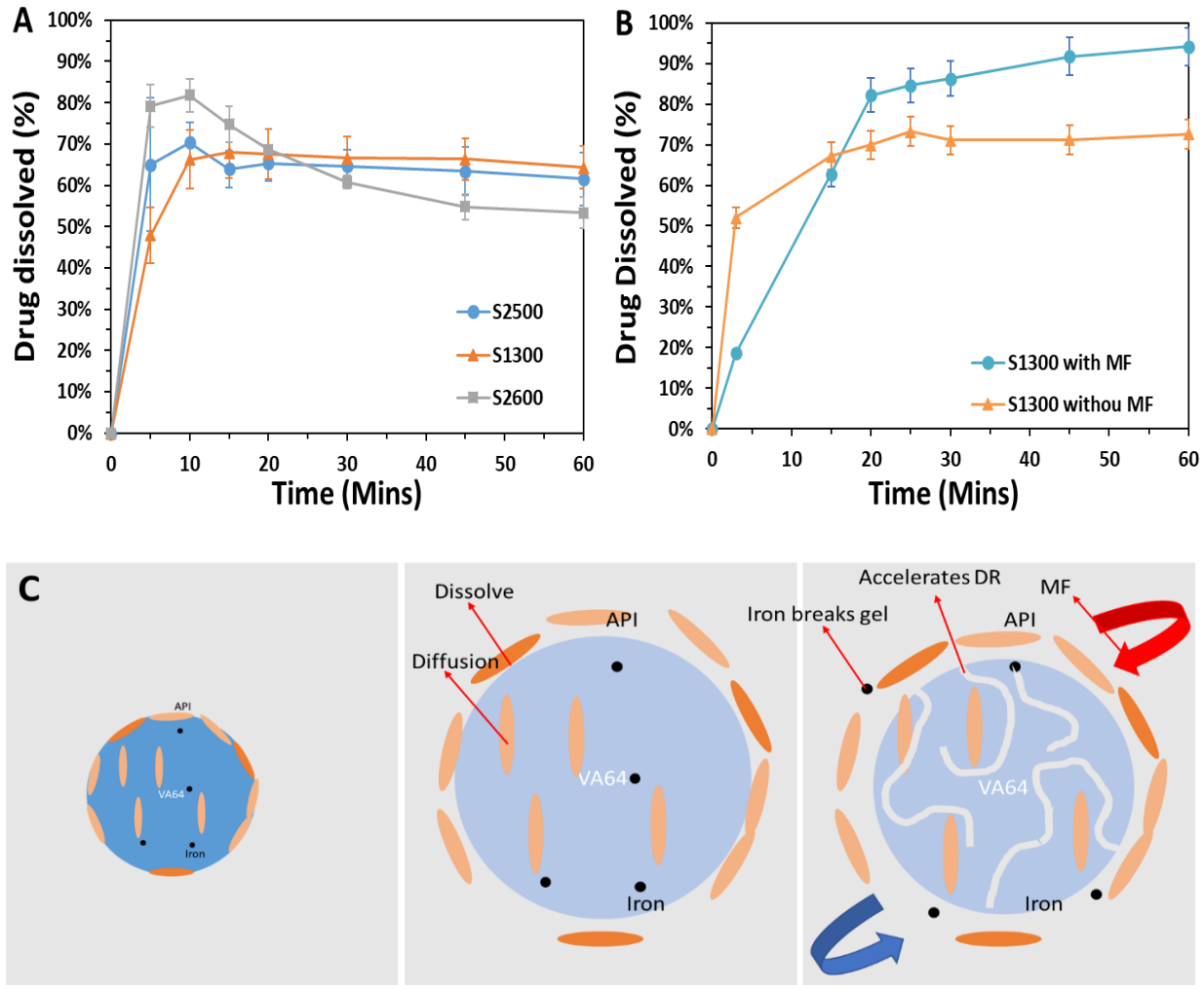

Figure 9. Dissolution profiles of Kollidon VA 64 based formulation, A)S1300, S2500, S2600, B) S1300 samples with and without magnetic stimuli. C) Schematic images of the magnetic field triggered drug release system.

6. Conclusion

An advanced drug formulation that contains carbonyl iron for making pharmaceutical tablets by using the SLS 3D printing method was successfully manufactured. Carbonyl iron not only absorbed the laser energy that helped with the sintering of the tablets, but also helped to improve the release of the drug under the magnetic field by harnessing its magnetism. Furthermore, carbonyl iron is an FDA-approved iron supplement. When

patients take the tablets, it helps them to replenish the daily required iron as well (18). Simultaneously, SLS 3D printing provides a novel way to prepare an oral pharmaceutical dosage form in a single step. This method also provides a facile approach to tailor the quality of tablets by adjusting the tablet formulations as well as the printing parameters. This is achieved by adjusting the laser scanning speed, the hatching spacing, and the internal temperature. Ultimately, this concept can be adapted for customized drug performance applications that depend on the requirements of the patient.

7. Acknowledgments

The research work reported herein was supported by Maniruzaman's start-up funds at The University of Texas at Austin and Faculty Science and Technology Acquisition and Retention (STARs) Award.

8. References

1. Smith DM, Kapoor Y, Klinzing GR, Procopio AT. Pharmaceutical 3D printing: Design and qualification of a single step print and fill capsule. Int J Pharm [Internet]. 2018;544(1):21–30. Available from: http://www.sciencedirect.com/science/article/pii/S0378517318302035

2. Thakkar R, Pillai AR, Zhang J, Zhang Y, Kulkarni V, Maniruzzaman M. Novel On-Demand 3-Dimensional (3-D) Printed Tablets Using Fill Density as an Effective Release-Controlling Tool. Vol. 12, Polymers. 2020.

3. Leong KF, Phua KKS, Chua CK, Du ZH, Teo KOM. Fabrication of porous polymeric matrix drug delivery devices using the selective laser sintering technique. Proc Inst Mech Eng Part H J Eng Med [Internet]. 2001 Feb 1;215(2):191–2. Available from: https://doi.org/10.1243/0954411011533751

4. Wang J, Goyanes A, Gaisford S, Basit AW. Stereolithographic (SLA) 3D printing of oral modified-release dosage forms. Int J Pharm [Internet]. 2016;503(1):207–12. Available from: http://www.sciencedirect.com/science/article/pii/S0378517316302150

5. McCarthy EM. Injection Molding Behavior of Novel Biocompatible Materials for Hard Tissue Engineering and Pharmaceutical Applications [Internet]. ProQuest Dissertations and Theses. [Ann Arbor]: University of Massachusetts Lowell; 2020. Available from: http://ezproxy.lib.utexas.edu/login?url=https://www.proquest.com/docview/2415349734?accountid=7118

6. Melocchi A, Loreti G, Del Curto MD, Maroni A, Gazzaniga A, Zema L. Evaluation of Hot-Melt Extrusion and Injection Molding for Continuous Manufacturing of Immediate-Release Tablets. J Pharm Sci [Internet]. 2015;104(6):1971–80. Available from: http://www.sciencedirect.com/science/article/pii/S0022354915300745

7. Wang Y, Xu Z, Wu D, Bai J. Current Status and Prospects of Polymer Powder 3D Printing Technologies. Vol. 13, Materials. 2020.

8. Olejarczyk M, Gruber P, Ziółkowski G. Capabilities and Limitations of Using Desktop 3-D Printers in the Laser Sintering Process. Appl Sci [Internet]. 2020;10(18):6184. Available from: http://ezproxy.lib.utexas.edu/login?url=https://www.proquest.com/docview/2441375858?accountid=7118

9. Davis DA, Thakkar R, Su Y, Williams RO, Maniruzzaman M. Selective Laser Sintering 3-Dimensional Printing as a Single Step Process to Prepare Amorphous Solid Dispersion Dosage Forms for Improved Solubility and Dissolution rate. J Pharm Sci [Internet]. 2020; Available from: http://www.sciencedirect.com/science/article/pii/S0022354920307413

10. Florencia EW, Novella S, Kah FL, Chee KC, E. WC, Chian CC. Selective laser sintering adaptation tools for cost effective fabrication of biomedical prototypes. Rapid Prototyp J [Internet]. 2010 Jan 1;16(2):90–9. Available from: https://doi.org/10.1108/13552541011025816

11. K.H. L, K.F. L, C.K. C, Z.H. D, C.M. C. Characterization of SLS parts for drug delivery devices. Rapid Prototyp J [Internet]. 2001 Jan 1;7(5):262–8. Available from: https://doi.org/10.1108/13552540110410468

12. Beaman JJ, Deckard CR. Selective Laser Sinterng With Assisted Powder Handlng [Internet]. Google Patents. 1990. p. 17. Available from: https://patents.google.com/patent/US4938816A/en%0Ahttps://patentimages.storage.googleapis.com/bf/cb/03/4cbcb828f78e25/US4938816.pdf

13. Fina F, Gaisford S, Basit AW. Powder Bed Fusion: The Working Process, Current

Applications and Opportunities BT - 3D Printing of Pharmaceuticals. In: Basit AW, Gaisford S, editors. Cham: Springer International Publishing; 2018. p. 81–105. Available from: https://doi.org/10.1007/978-3-319-90755-0_5

14. Calignano F, Galati M, Iuliano L, Minetola P. Design of Additively Manufactured Structures for Biomedical Applications: A Review of the Additive Manufacturing Processes Applied to the Biomedical Sector. J Healthc Eng. 2019;2019:6.

15. Barakh Ali SF, Mohamed EM, Ozkan T, Kuttolamadom MA, Khan MA, Asadi A, et al. Understanding the effects of formulation and process variables on the printlets quality manufactured by selective laser sintering 3D printing. Int J Pharm [Internet]. 2019;570:118651. Available from: http://www.sciencedirect.com/science/article/pii/S0378517319306969

16. Japka JE. Microstructure and Properties of Carbonyl Iron Powder. JOM [Internet]. 1988;40(8):18–21. Available from: https://doi.org/10.1007/BF03258115

17. Zhu Q, Qian Y, Yang Y, Wu W, Xie J, Wei D. Effects of carbonyl iron powder on iron deficiency anemia and its subchronic toxicity. J Food Drug Anal [Internet]. 2016 Oct;24(4):746–53. Available from: http://10.0.3.248/j.jfda.2016.04.003

18. Antonio S, Wabner CL, Lake C, Alexandrides G. Dietary supplements containing ultradense calcium citrate and carbonyl iron. Vol. 1. 2004.

19. Whittaker P, Ali SF, Imam SZ, Dunkel VC. Acute Toxicity of Carbonyl Iron and Sodium Iron EDTA Compared with Ferrous Sulfate in Young Rats. Regul Toxicol Pharmacol [Internet]. 2002;36(3):280–6. Available from: http://www.sciencedirect.com/science/article/pii/S0273230002915771

20. Fina F, Goyanes A, Gaisford S, Basit AW. Selective laser sintering (SLS) 3D printing of

medicines. Int J Pharm [Internet]. 2017;529(1):285–93. Available from: http://www.sciencedirect.com/science/article/pii/S0378517317305902

21. Fina F, Madla CM, Goyanes A, Zhang J, Gaisford S, Basit AW. Fabricating 3D printed orally disintegrating printlets using selective laser sintering. Int J Pharm [Internet]. 2018;541(1):101–7. Available from: http://www.sciencedirect.com/science/article/pii/S0378517318300966

22. Shirazi SFS, Gharehkhani S, Mehrali M, Yarmand H, Metselaar HSC, Adib Kadri N, et al. A review on powder-based additive manufacturing for tissue engineering: selective laser sintering and inkjet 3D printing. Sci Technol Adv Mater [Internet]. 2015 Jun 20;16(3):33502. Available from: https://doi.org/10.1088/1468-6996/16/3/033502

23. Charoo NA, Barakh Ali SF, Mohamed EM, Kuttolamadom MA, Ozkan T, Khan MA, et al. Selective laser sintering 3D printing – an overview of the technology and pharmaceutical applications. Drug Dev Ind Pharm [Internet]. 2020 Jun 2;46(6):869–77. Available from: https://doi.org/10.1080/03639045.2020.1764027

24. Awad A, Fina F, Goyanes A, Gaisford S, Basit AW. 3D printing: Principles and pharmaceutical applications of selective laser sintering. Int J Pharm [Internet]. 2020;586:119594. Available from: http://www.sciencedirect.com/science/article/pii/S0378517320305780

25. Awad A, Yao A, Trenfield SJ, Goyanes A, Gaisford S, Basit AW. 3D Printed Tablets (Printlets) with Braille and Moon Patterns for Visually Impaired Patients. Pharmaceutics [Internet]. 2020 Feb 19;12(2):172. Available from: https://pubmed.ncbi.nlm.nih.gov/32092945

26. Awad A, Fina F, Trenfield JS, Patel P, Goyanes A, Gaisford S, et al. 3D Printed Pellets

(Miniprintlets): A Novel, Multi-Drug, Controlled Release Platform Technology. Vol. 11, Pharmaceutics. 2019.

27. Mohamed EM, Barakh Ali SF, Rahman Z, Dharani S, Ozkan T, Kuttolamadom MA, et al. Formulation Optimization of Selective Laser Sintering 3D-Printed Tablets of Clindamycin Palmitate Hydrochloride by Response Surface Methodology. AAPS PharmSciTech [Internet]. 2020;21(6):232. Available from: https://doi.org/10.1208/s12249-020-01775-0